Enhanced Rotational Dynamics of the Phosphorylation Domain of the Ca-ATPase upon Calcium Activation†

Shaohui Huang and Thomas C. Squier*

Biochemistry and Biophysics Section, Department of Molecular Biosciences, University of Kansas, Lawrence, Kansas 66045-2106

Received August 18, 1998; Revised Manuscript Received November 3, 1998

ABSTRACT: We have used labeling conditions that permit the specific and covalent attachment of erythrosin isothiocyanate (Er-ITC) to Lys_{464} within the phosphorylation domain of the Ca-ATPase in skeletal sarcoplasmic reticulum membranes. These labeling conditions do not interfere with high-affinity ATP binding, phosphoenzyme formation, or phosphoenzyme hydrolysis [Huang, S., Negash, S., and Squier, T. C. (1998) *Biochemistry 37,* 6949−6957]. Thus, we can use frequency-domain phosphorescence spectroscopy to measure the rotational dynamics of the Ca-ATPase stabilized in different enzymatic states corresponding to the absence of bound ligands (E), calcium activation (E·Ca_2), the presence of bound nucleotide (E·ATP), and formation of phosphoenzyme (E−P). We resolve three rotational correlation times corresponding to (i) a large-amplitude domain motion of the phosphorylation domain ($\phi_1 \approx 5 \pm 1$ μs), (ii) overall protein rotational motion with respect to the membrane normal ($\phi_2 \approx 50 \pm 10$ μs), and (iii) the rotational motion of the SR vesicles ($\phi_3 \approx 1.1 \pm 0.4$ ms). No differences are observed in the rotational dynamics of E, E·ATP, or E−P, indicating that phosphoenzyme formation or nucleotide binding result in no global structural changes involving the phosphorylation domain. In contrast, calcium activation enhances the amplitude of motion of the phosphorylation domain. These observed calcium-dependent changes in rotational dynamics result from structural changes within a single Ca-ATPase polypeptide chain, since protein−protein interactions do not change upon calcium binding. Thus, calcium binding induces concerted domain motions within a single Ca-ATPase polypeptide chain that may play a critical role in facilitating substrate binding and utilization.

The Ca-ATPase present in sarcoplasmic reticulum (SR)[1] membranes functions to re-sequester calcium ions following excitation−contraction coupling, and normally represents the rate-limiting step associated with muscle contraction (*1*). The vectorial transport of calcium involves the structural coupling between the spatially distant nucleotide and calcium binding sites, found respectively in the cytoplasmic region and transmembrane helices (*2*). The cytoplasmic portion of the Ca-ATPase contains multiple domains whose relative orientation with respect to one another has been suggested to be important to catalytic function due to (i) sequence homology with water-soluble kinases and (ii) large differences in the tertiary structures of the cytoplasmic domains of the Ca-ATPase or homologous H^+-ATPase determined under conditions expected to stabilize different enzymatic states (*3*−*9*). Thus, the H^+-ATPase crystallized in an unliganded form or the Ca-ATPase in the presence of millimolar calcium contains considerable electron density near the membrane surface and exhibits a relatively open conformation (*8*, *9*). In contrast, tubular crystals of the Ca-ATPase stabilized in a conformation thought to mimic the phosphoenzyme intermediate obtained in the presence of decavanadate demonstrate a narrow stalklike region connecting the cytosolic regions to the transmembrane helices (*5*, *7*). These results suggest that large structural rearrangements involving cytoplasmic domains of the Ca-ATPase may facilitate ion translocation. However, the relationship between the resolved structures and physiological states of the Ca-ATPase remains uncertain due to the presence of multiple forms of vanadate in the crystallization medium or the binding of calcium to low-affinity sites. To identify structural differences between cytoplasmic domains of the Ca-ATPase under more physiological conditions, we have used frequency-domain phosphorescence spectroscopy to measure the rotational dynamics of the phosphorylation domain of the Ca-ATPase covalently modified at Lys_{464} with erythrosin isothiocyanate, which possesses long-lived excited states approaching the turnover number of the Ca-ATPase (*4*, *6*, *10*−*12*). Under these labeling conditions the Ca-ATPase remains catalytically active (*12*), permitting the measurement of dynamic structural changes of the phosphorylation domain within a functional Ca-ATPase stabilized in different enzymatic states.

† Supported by NIH Grant GM46837.

* Correspondence should be addressed to this author. Telephone: (785)-864-4008. FAX: (785)-864-5321. E-mail: TCSQUIER@KUHUB.CC.UKANS.EDU.

[1] Abbreviations: ATP, adenosine 5′-triphosphate; BSA, bovine serum albumin; $C_{12}E_8$, polyoxyethylene 8-lauryl ether; DPH-PC, 2-[3-(diphenylhexatrienyl) propanoyl]-1-hexadecanoyl-*sn*-glycero-3-phosphocholine; EGTA, ethylene glycol bis(β-aminoethyl ether)-*N*,*N*,*N*′,*N*′-tetraacetic acid; Er-IA, erythrosin 5-iodoacetamide; Er-ITC, erythrosin 5-isothiocyanate; FD, frequency-domain; FITC, fluorescein 5-isothiocyanate; FRET, fluorescence resonance energy transfer; MOPS, 3-(*N*-morpholino)propanesulfonic acid; *P*, polarization; PAL, protein-associated phospholipid; SR, sarcoplasmic reticulum; Texas Red, sulforhodamine B.

10.1021/bi981997+ CCC: $15.00
Published on Web 12/03/1998

EXPERIMENTAL PROCEDURES

Materials. KCl was purchased from Research Organics (Cleveland, OH). Sucrose, TRIS (free base), and MOPS [3-(*N*-morpholino)propanesulfonic acid] were obtained from Fisher Scientific (Pittsburgh, PA). $CaCl_2$ standard solution was from VWR (St. Louis, MO). A23187, ammonium molybdate, ATP (disodium salt), isomer II of erythrosin 5-isothiocyanate (Er-ITC), erythrosin 5-iodoacetamide (Er-IA), EGTA, isomer I of fluorescein 5-isothiocyanate (FITC), β-D(+)-glucose, $MgCl_2$, and sulforhodamine B (Texas Red) were from Sigma (St. Louis, MO). Polyoxyethylene 8-lauryl ether ($C_{12}E_8$) was from Nikkol Co. (Tokyo, Japan). Bovine serum albumin (BSA), glucose oxidase, and catalase were from Worthington (Freehold, NJ). 2-[3-(Diphenylhexatrienyl)propanoyl]-1-hexadecanoyl-*sn*-glycero-3-phosphocholine (DPH-PC) was obtained from Avanti (Alabaster, AL). SR membranes were isolated from rabbit fast-twitch skeletal muscle, essentially as previously described (*13*). SR lipids were extracted as previously described (*14*, *15*). All samples were stored in 20 mM MOPS (pH 7.0) and 0.3 M sucrose at −70 °C.

Derivatization of Samples with Optical Probes. Er-ITC was covalently bound to Lys_{464} on the Ca-ATPase at a stoichiometry of approximately 1 nmol of Er-ITC bound/mg of SR membranes, as previously described in detail (*12*). Lys_{515} within the Ca-ATPase was labeled with FITC as previously described (*16*). Sulfhydryls in BSA (10 mg mL^{-1}) were derivatized with 70 μM Er-IA in 30 mM MOPS (pH 7.5), 5 mM $MgCl_2$, and 0.1 M KCl at 25 °C for 15 min, resulting in the incorporation of 0.15 mol of Er-IA/mol of BSA.

Incorporation of DPH-PC into Membranes. DPH-PC was incorporated into SR membranes by incubating 50 μM DPH-PC with 5 mg mL^{-1} SR membranes in 50 mM MOPS (pH 7.0) overnight on ice, followed by centrifugation to remove unincorporated DPH-PC. Alternatively, DPH-PC was added to SR lipids dissolved in $CHCl_3$ at a molar ratio of 1:100; lipids were dried overnight under a vacuum, and vesicles were formed by bath sonication in 50 mM MOPS (pH 7.0) and 10% (w/v) sucrose for 30 min. Large aggregates were removed by ultracentrifugation, essentially as previously described (*17*).

Enzymatic Activity Assays. The rate of ATP hydrolysis was measured as an ammonium molybdate complex of phosphate (*18*). Measurements of total and calcium-independent ATPase activity involved the addition of the indicated concentration of an equimolar solution of $MgCl_2$ and ATP to 0.02 mg mL^{-1} SR vesicles in a medium containing 35 mM MOPS (pH 7.0), 100 mM KCl, 5 mM $MgCl_2$, 4 μM A23187, and either 100 μM $CaCl_2$ or 2 mM EGTA at 25 °C.

Diameter of SR Vesicles. The average diameter of SR vesicles was measured using a Nicomp 370 submicron particle sizer dynamic (Santa Barbara, CA), and the distribution of vesicle sizes was fit to a Gaussian distribution (*19*).

Phosphorescence Measurements. Approximately 1 mW of 514 nm modulated light from an argon ion laser (Coherent Corp., Palo Alto, CA) was used to excite (i) Er-ITC-derivatized SR vesicles (0.3 mg/mL) suspended in buffer A [35 mM MOPS (pH 7.0), 0.1 M KCl, 5 mM $MgCl_2$, and 0.3 M sucrose] or buffer B [20 mM MES (pH 6.0), 20 mM $MgCl_2$, 20 mM K_2HPO_4, and 0.3 M sucrose] in the presence of 100 μM $CaCl_2$ or 200 μM EGTA or (ii) Er-IA-labeled BSA (0.5 mg/mL) in 20 mM MOPS (pH 7.0) and 90% (w/w) glycerol. The phosphorescence emission was collected following a Schott RG697 long-pass filter (Figure 1A). Prior to the measurement of phosphorescence, the concentration of dissolved oxygen was reduced enzymatically by the addition of 17 mM glucose, 3 units of glucose oxidase activity, and 30 units of catalase activity, and subsequent incubation in the dark for at least 5 min (*20*). Independent oximetry measurements involving spin-label EPR spectroscopy were performed as previously described (*21*), and indicate that the concentration of dissolved oxygen was less than 70 μM under these conditions. Phosphorescence lifetime and anisotropy measurements were performed using an ISS K2 frequency-domain fluorometer (ISS Corp., Champaign, IL). The intensity of the excitation laser was modulated with a Pockels cell coupled to a frequency generator (Marconi Instruments LTD, Stevenage, Hertz, U.K.) and an ISS K2.LF low-frequency modulator. To avoid color effects, lifetime measurements were made in the ratio mode, using Texas Red ($<\tau> = 2$ ns) dissolved in methanol as the reference. The quantum yield of Er-ITC bound to the Ca-ATPase in buffer A and 0.1 mM $CaCl_2$ was determined to be 0.02 using fluorescein as a reference, which has a quantum yield of 0.85 (*22*).

Fluorescence Measurements. Excitation of FITC-derivatized SR membranes (0.05 mg/mL) suspended in buffer A and 100 μM $CaCl_2$ involved the 493 nm line of an argon ion laser (Coherent Corp.), and emitted fluorescence was detected after a Schott OG-530 long-pass filter using a Glan−Thompson polarizer set parallel or perpendicular to the vertically polarized excitation light. Excitation of DPH-PC (2 μM) in SR membranes (0.2 mg mL^{-1}) or in vesicles made from extracted SR lipids (200 μM) involved excitation at

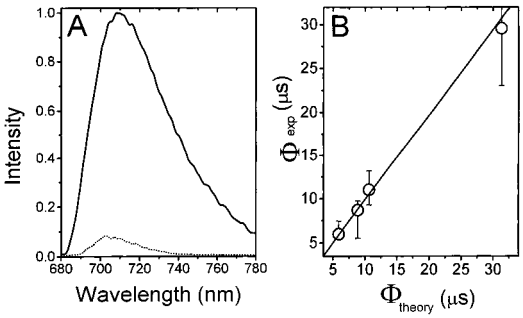

FIGURE 1: Phosphorescence emission spectra and sensitivity to microsecond rotational dynamics. (A) Emission spectra are shown for Er-ITC-modified Ca-ATPase (0.3 mg mL^{-1}) at 25 °C in the absence (dotted line) or presence (solid line) of 3 units of glucose oxidase, 30 units of catalase, and 17 mM glucose. (B) Comparison of the measured (ϕ_{exp}) and theoretical (ϕ_{theory}) rotational correlation times for Er-IA-labeled BSA in 90% (w/w) glycerol assuming the Stokes−Einstein equation (*91*), where $\phi_{theory} = 1/6D_r = V\eta/kT$. D_r is the rotational diffusion coefficient of BSA, V is the volume (110.4 nm^3) assuming 34% hydration (*92*), η is the viscosity in Poise, k is Boltzmann's constant, and T is the absolute temperature in degrees Kelvin. The temperature was varied from 2, 13, 15, and 20 °C; the corresponding viscosities of 90% (w/w) glycerol (in Poise) were 10.7, 3.8, 3.2, and 2.2 (*93*). Error bars represent one standard deviation, and were determined from a Global analysis of the data using the *F*-statistic (*30*). A line with a slope of 1.0 is drawn to facilitate comparison. A least-squares fit of the data yields a slope of 0.93 ± 0.01.

351 nm, and the fluorescence was detected after a Corning 3-73 long-pass filter. Lifetime and anisotropy measurements were made using an ISS-K2 fluorometer (see above), and data were fit using frequency-independent errors of 0.2° for the phase and 0.02 for the modulation, as previously described (*17*).

Data Analysis. Decreases in the emission anisotropy [$A = (1/P - 1/3)^{-1}$] of FITC bound to the Ca-ATPase upon increasing the labeling stoichiometry result from fluorescence resonance energy transfer (FRET), and provide information regarding subunit interactions between neighboring Ca-ATPase polypeptide chains (*23*−*25*), where

$$A(A_o,A_s,A_t) = \sum_{r=1}^{N} \frac{(N-1)!}{(r-1)!(N-r)!}(f)^{r-1}(1-f)^{N-r} \times \left[A_o - (A_o - A_s)\frac{\frac{(r-1)(A_o - A_s)}{(N-1)(A_s - A_t)}}{1 + \frac{(r-1)(A_o - A_s)}{(N-1)(A_s - A_t)}}\right] \quad (1)$$

$A(A_o,A_s,A_t)$ is the measured emission anisotropy, f is the labeling stoichiometry of FITC per mole of Ca-ATPase, N is the apparent oligomeric state of the Ca-ATPase, A_o is the initial emission anisotropy in the absence of FRET, A_s is the emission anistropy when all FITC labeling sites within the Ca-ATPase oligomeric complex are saturated, and A_t is the emission anisotropy after one FRET event. Fitting the data involves incrementally adjusting N by integral values and solving for A_o, A_s, and A_t, which provide information regarding both the spatial separation and the orientation of chromophores on adjacent Ca-ATPase polypeptide chains (*23*, *24*). In the presence of a heterogeneous population of Ca-ATPase polypeptides with the two known oligomeric states N_a and N_b, the fractional contribution of each species can be determined from

$$A_{observed} = [f_a \times A_a(N_a)] + [(1 - f_a) \times A_b(N_b)] \quad (2)$$

Phosphorescence intensity or anisotropy decays were fit to a sum of exponentials using the method of nonlinear least-squares using explicit expressions that permit the calculation of the lifetime components for a multiexponential decay (α_i and τ_i). Alternatively, appropriate expressions have been derived that permit determination of the initial anisotropy (r_0), the rotational correlation times (ϕ_i), and the amplitudes of the total anisotropy loss associated with each rotational correlation time ($r_0 g_i$). The derivation and application of these expression have previously been described in detail (*26*−*28*). Data were fit using the Globals software package (University of Illinois, Urbana−Champaign). Unless otherwise indicated, data were analyzed using frequency-independent errors in the phase and modulation that were assumed to be 0.2° and 0.005, respectively.

RESULTS

Frequency-Domain Phosphorescence Anisotropy Measurements of Microsecond Rotational Dynamics. In contrast to the widespread use of frequency-domain (FD) methods in fluorescence spectroscopy (*29*), there are currently limited examples in which FD phosphorescence measurements have been used to investigate the microsecond rotational dynamics of biological macromolecules. Therefore, to ensure the reliability of the FD phosphorescence technique in the measurement of microsecond rotational dynamics, we have compared the theoretical rotational correlation time calculated from the Stokes−Einstein equation (see legend to Figure 1) with the measured rotational correlation time of a model protein, BSA, covalently modified with erythrosin iodoacetamide (Er-IA).

The rotational dynamics of Er-IA-labeled BSA in 90% (w/w) glycerol were measured between 3 and 20 °C, where the differential phase and modulated anisotropy data at each of 4 temperatures were collected at 17 modulation frequencies between 0.1 and 20 kHz. Data were fit using the method of nonlinear least-squares to a sum of exponentials (*30*). In all cases, the rotational dynamics of BSA were best described by two rotational correlation times, i.e., 0.5 and 8.7 μs at 15 °C. The larger rotational correlation time agrees with earlier measurements of the global rotational motion of BSA (*31*). The smaller rotational correlation time (0.5 μs) probably reflects domain motion within BSA (*32*). In all cases the larger rotational correlation time, whose preexponential amplitude was 0.76 at 15 °C, dominates the phosphorescence anisotropy decay. At all four temperatures, the measured (ϕ_{exp}) and calculated (ϕ_{theory}) rotational correlation times agree (Figure 1B), indicating that FD phosphorescence anisotropy measurements accurately measure the microsecond rotational dynamics of proteins.

Measurement of the Phosphorescence Lifetimes and Rotational Dynamics of Er-ITC-Labeled Ca-ATPase. We have selectively labeled Lys_{464} within an ATP protectable site on the cytoplasmic domain of the Ca-ATPase, using conditions that have previously been shown to preserve the catalytic activity associated with high-affinity nucleotide binding (*12*). To minimize FRET between Er-ITC molecules, we used less than stoichiometric amounts of Er-ITC (approximately 1 nmol mg^{-1} SR protein) bound to the Ca-ATPase (approximately 4 nmol mg^{-1} SR protein) (*33*). Thus, global structural changes of the phosphorylation domain can be measured using equilibrium conditions that stabilize different enzymatic states.

FD measurements of the rotational dynamics of the Ca-ATPase require the measurement of the phosphorescence lifetime. Therefore, the frequency response of the phase delay and modulation of Er-ITC bound to the Ca-ATPase was measured at 20 frequencies between 0.1 and 100 kHz (Figure 2A). The intensity decay of Er-ITC bound to the Ca-ATPase can be adequately described as a sum of four exponentials, as shown by the random distribution of the weighted residuals (Figure 2E). The average phosphorescence lifetime of Er-ITC bound to the Ca-ATPase is 320 ± 60 μs at 25 °C (Table 1), which is sufficiently long to enable the measurement of internal domain motions and the overall uniaxial rotational motion of the Ca-ATPase with respect to the membrane normal (*34*, *35*).

Resolution of the rotational dynamics of Er-ITC bound to the Ca-ATPase involved the measurement of the differential phase and modulated anisotropy between 0.2 and 20 kHz (Figure 3). The frequency-domain anisotropy data can be adequately described as a sum of three exponentials, as

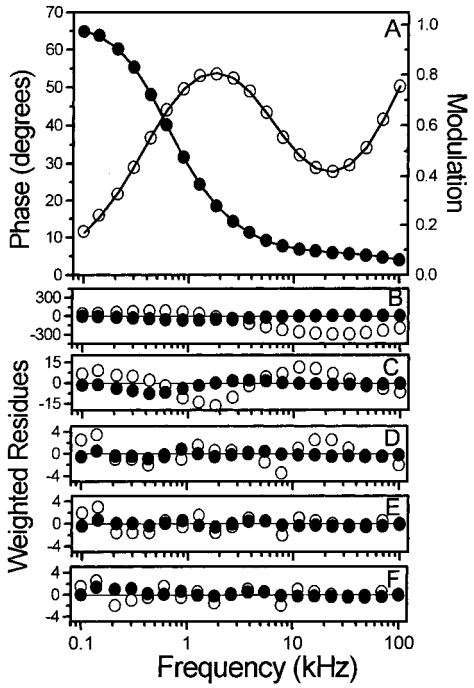

FIGURE 2: Phosphorescence lifetime data for Er-ITC bound to the Ca-ATPase. (A) Frequency-responses and multiexponential fits to a sum of four exponentials are shown corresponding to phase shift (○) and modulation (●) for Er-ITC bound to the Ca-ATPase in native sarcoplasmic reticulum vesicles. Weighted residuals are shown for the fits to the (B) one-, (C) two-, (D) three-, (E) four-, and (F) five-exponential functions, respectively. The corresponding χ^2_R values for these fits were 16 400, 40, 1.8, 0.9, and 0.8. Experimental conditions involved 0.3 mg mL^{-1} Er-ITC-modified Ca-ATPase in buffer A in the presence of 0.1 mM $CaCl_2$, 3 units of glucose oxidase, 30 units of catalase, and 17 mM glucose at 25 °C. Frequency-domain errors in the measurement of the phase shift and modulation were 0.2° and 0.005, respectively.

shown by the randomly weighted residuals (Figure 3E; Table 2). The fit to the three-exponential model is superior to a model involving two rotational correlation times and a residual anisotropy, which is characterized by a 2-fold larger χ^2_R and nonrandom residuals (data not shown). The initial anisotropy ($r_0 = 0.37 \pm 0.03$; Table 2) is close to the theoretical maximum of 0.4, indicating that we have resolved the majority of the phosphorescence anisotropy decay, and that Er-ITC is rigidly bound to Lys_{464} (*36*−*40*). Thus, the specificity of labeling and the time-scale of motion are appropriate for the detection of global structural rearrangements that may be involved in the catalytic cycle of the Ca-ATPase.

Calcium-Induced Dynamic Structural Changes of the Phosphorylation Domain. Global structural rearrangements involving domain motions within the Ca-ATPase that accompany the transport cycle of the Ca-ATPase were measured for the Er-ITC-labeled Ca-ATPase under equilibrium conditions that stabilize different enzymatic intermediates (*41*, *42*). These conditions involve (i) the absence of a bound ligand (E), (ii) calcium activation ($E{\cdot}Ca_2$), (iii) the presence of a bound nucleotide (E·ATP), and (iv) formation of phosphoenzyme (E−P). In all cases the data are adequately described by a model involving three rotational correlation times (see above). Calcium activation results in substantial differences in the modulated anisotropy and differential phase shifts compared with any of the other enzyme intermediates (Figure 4). Similar calcium-dependent increases in the rotational dynamics are observed upon the addition of either 10 or 100 μM $CaCl_2$, indicating that the observed structural changes are the result of specific binding to the high-affinity calcium sites. A consideration of the fitting parameters obtained for each catalytic intermediate indicates that the increase in the rotational dynamics of the Ca-ATPase associated with calcium activation primarily results from an increase in the amplitude (g_1r_0) associated with ϕ_1, without significant changes in any of the rotational correlation times (Table 3). The increase in the average lifetime of the calcium-activated enzyme at pH 7.0 suggests that calcium activation results in a decreased polarity in the vicinity of bound Er-ITC at Lys_{464} (Table 3).

Physical Significance of Measured Rotational Correlation Times. The physical basis of the observed rotational correlation times ($\phi_1 = 5 \pm 1$ μs, $\phi_2 = 50 \pm 10$ μs, and $\phi_3 = 1.1 \pm 0.4$ ms; Tables 2 and 3) can be appreciated by comparison with rotational correlation times calculated for specific models. For example, a rotational correlation time of SR vesicles can be calculated from the Stokes−Einstein equation if the diameter of the vesicles is known. Using dynamic light scattering, the measured mean radius of SR vesicles is 98 ± 9 nm, permitting the calculation of their volume as $(4 \pm 1) \times 10^6$ nm^3. Thus, the expected rotational correlation time for SR vesicles in 10% (w/v) sucrose at 25 °C ($\eta = 1.18$ cP; *43*) can be calculated to be 1.1 ± 0.4 ms, in good agreement with the longest component of the measured rotational correlation times ($\phi_3 = 1.1 \pm 0.4$ ms; Tables 2 and 3); these results are consistent with an assignment of ϕ_3 as the overall rotational motion of SR vesicles.

The expected rotational correlation time (ϕ_{theory}) of the Ca-ATPase relative to the membrane normal can be calculated from the overall dimensions of the transmembrane portion of the Ca-ATPase and the viscosity (η) of the SR membrane, previously determined as 3.7 P at a temperature (T) of 25 °C (*35*, *44*), where

$$\phi_r = \frac{2\pi\eta h(a^2 + b^2)}{k \times T} \quad (3)$$

The structure of the Ca-ATPase has been solved at 8 Å resolution (*5*, *7*). The height (h) of the transmembrane helices is 3.2 nm, and the cross-sectional area of the transmembrane helices relative to the membrane normal can be approximated as an ellipse whose major (a) and minor (b) axes are 3.0 and 2.0 nm, respectively. Thus, the expected rotational correlation time for a monomeric form of the Ca-ATPase in SR lipids is about 24 μs. However, the Ca-ATPase has been suggested to function as a dimer within the SR membrane (*42*, *45*−*49*). While the relative orientation of Ca-ATPase polypeptide chains with respect to one another is unclear within native SR membranes, the structure of tubular crystals of the Ca-ATPase suggests the major axis (a) to be approximately 5.5 nm (*5*). Thus, the estimated rotational correlation time for such a dimer is 62 μs, which is similar to that observed for the Er-ITC labeled Ca-ATPase ($\phi_2 = 50 \pm 10$ μs; Table 2). The smallest rotational correlation time ($\phi_1 = 5 \pm 1$ μs; Tables 2 and 3) is therefore too short to correspond to uniaxial rotational motion of the entire Ca-ATPase polypeptide chain. However, ϕ_1 is longer than

Table 1: Phosphorescence Intensity Decay Parameters of ErITC-Labeled Ca-ATPase[a]

f_1	τ_1 (μs)	f_2	τ_2 (μs)	f_3	τ_3 (μs)	f_4	τ_4 (μs)	$<\tau>^b$ (μs)	χ_R^2
1.0	130 (120)							130 (120)	16358
0.09 (0.01)	1.8 (0.1)	0.91 (0.01)	320 (20)					290 (20)	40
0.09 (0.01)	1.7 (0.1)	0.06 (0.02)	80 (10)	0.85 (0.02)	360 (10)			310 (10)	1.8
0.08 (0.04)	1.7 (0.1)	0.01 (0.01)	20 (10)	0.08 (0.08)	110 (30)	0.83 (0.05)	370 (70)	320 (60)	0.9

[a] Measurements involved 0.3 mg mL^{-1} SR vesicles in buffer A and 100 μM $CaCl_2$ at 25 °C. Parameters are derived from a nonlinear least-squares fit of the data to multiexponential decay models: $I(t) = \sum\alpha_i e^{-t/\tau}$ (*29*). Numbers in parentheses are the maximal variance associated with one standard deviation determined from a Global analysis of the data (*30*). [b] $<\tau> = \sum f_i\tau_i$ where $f_i = \alpha_i\tau_i/\sum\alpha_i\tau_i$.

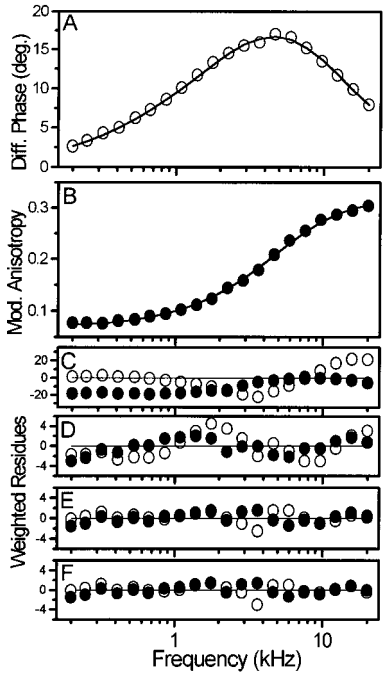

FIGURE 3: Frequency-domain phosphorescence anisotropy data for Er-ITC bound to the Ca-ATPase. Differential phase angle (A) and modulated anisotropy (B) of Er-ITC-labeled Ca-ATPase with superimposed fits to a model involving three exponentials. Weighted residuals are shown for the (C) one-, (D) two-, (E) three-, and (F) four-exponential fits to the data, assuming frequency-independent errors in the measurement of the differential phase and modulated anisotropy of 0.2° and 0.005. The corresponding χ^2_R values for these fits were 171, 4.0, 1.0, and 1.0, respectively. Experimental conditions are as described in the legend to Figure 2.

domain motions observed for proteins in aqueous medium which generally occur on the submicrosecond time scale (*10*, *37*). Thus, ϕ_1 likely corresponds to a restricted motion involving the cytosolic domain of the Ca-ATPase, whose rotational mobility is hindered by its linkage to transmembrane helices through the stalk region (*5*, *7*, *9*).

Correlation between Rotational Dynamics of the Ca-ATPase and Membrane Viscosity. Further substantiation of the physical significance of the observed rotational correlation times of Er-ITC-labeled Ca-ATPase is possible by considering the direct relationship between the rate of uniaxial rotational motion of the Ca-ATPase and membrane viscosity (η) (*44*, *50*, *51*). We have therefore compared the temperature dependence of the rotational dynamics of the Ca-ATPase and SR phospholipids; rotational correlation times (ϕ_1, ϕ_2, and ϕ_3) and associated amplitudes (r_0g_1, r_0g_2, and r_0g_3) of the Er-ITC-labeled Ca-ATPase are shown in Figure 5. As expected, the rotational correlation times associated with ϕ_2 and ϕ_3, assigned as overall rotational motion of the Ca-ATPase and SR vesicle tumbling, decreased with increasing temperature, indicating that the rates of their respective rotational motions increase. These rates of motion exhibit a linear Arrhenius relationship for ϕ_2 (Figure 6A) and ϕ_3 (data not shown), with respective activation energies of 5.6 ± 0.5 and 1.5 ± 0.5 kcal mol^{-1}. In contrast, the rotational correlation time associated with ϕ_1 increases with increasing temperature between 2 and 15 °C, is approximately constant between 15 and 25 °C, and finally decreases above 25 °C (Figure 5D). Thus, ϕ_1 is not directly related to changes in either overall protein rotational motion (i.e., ϕ_2) or membrane viscosity, which has been shown to have a linear Arrhenius dependence (*51*, *52*). Rather, we suggest that ϕ_1 corresponds to the rotational dynamics of the phosphorylation domain, whose structural elements include transmembrane helices involved in high-affinity calcium binding that may function to reduce the rate of domain motion (*7*). The decreased rate of motion between 2 and 15 °C suggests the presence of temperature-dependent structural rearrangements between cytosolic domains, consistent with earlier results that also reported a temperature-dependent change in the electron density profile of individual Ca-ATPase polypeptide chains (*53*). A similar temperature dependence is observed between ϕ_1 and phosphoenzyme formation from inorganic phosphate (*54*, *55*), suggesting that such structural changes may be critical to the formation of phosphoenzyme. This interpretation is consistent with the observation that phosphoenzyme formation is an entropy-driven process involving enhanced protein−protein interactions (*56*, *57*).

Additional support that the 50 μs rotational correlation time (i.e., ϕ_2; Tables 2 and 3) corresponds to the overall rotational motion of the Ca-ATPase with respect to the membrane normal comes from a quantitative consideration of the temperature dependence of membrane viscosity, which was measured using the fluorescent phospholipid analogue DPH-PC incorporated into (i) native SR membranes and (ii) in vesicles made from extracted SR lipids. The anisotropy decays of DPH-PC incorporated into either SR lipid vesicles or SR membranes were adequately described by two rotational correlation times (i.e., ϕ_{L1} and ϕ_{L2}) and a residual anisotropy (r_∞), which are associated with rapid intramolecular chain isomerization ($\phi_{L1} \approx 0.1$ ns), acyl chain reorientations about the bilayer normal ($\phi_{L2} \approx 4$ ns), and the order parameter of the phospholipid acyl chains (*17*, *58*). The rotational correlation times, residual anisotropy, and activation energy associated with phospholipid acyl-chain reorientation relative to the membrane normal (i.e., $1/\phi_{L2}$) are all larger in SR membranes ($r_\infty = 0.127$; $E_a = 4.4 \pm 0.5$ kcal mol^{-1}) relative to the vesicles made from SR lipids ($r_\infty = 0.073$; $E_a = 3.3 \pm 0.2$ kcal mol^{-1}) (Figure 6). These results are consistent with previous measurements indicating that the Ca-ATPase restricts the mobility of 43% of the phos-

Table 2: Phosphorescence Anisotropy Decay Parameters of the ErITC-Labeled SR[a]

r_0	g_1	ϕ_1 (μs)	g_2	ϕ_2 (μs)	g_3	ϕ_3 (μs)	χ_R^2
0.29 (0.04)	1.0	30 (10)					212
0.35 (0.02)	0.73 (0.02)	9 (1)	0.27 (0.02)	500 (100)			5.5
0.37 (0.03)	0.61 (0.04)	5 (1)	0.21 (0.03)	50 (10)	0.18 (0.02)	1100 (400)	0.9

[a] Measurements involved 0.3 mg mL^{-1} SR vesicles in buffer A and 100 μM $CaCl_2$ at 25 °C. Numbers in parentheses represent the maximal variance associated with one standard deviation obtained from a global analysis of the error surface (*30*). Parameter values were obtained by fitting the data to the equation:

$$A(t) = r_0 \sum_i g_i e^{-t/\phi_i}.$$

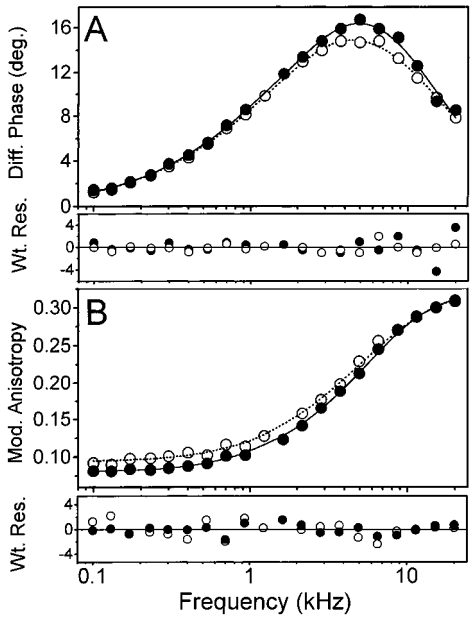

FIGURE 4: Enhanced microsecond rotational dynamics of the cytoplasmic domain of the Ca-ATPase upon calcium activation. Differential phase angle (A) and modulated anisotropy (B) are shown after either calcium activation (●) or phosphoenzyme formation (○). Weighted residuals are shown below the corresponding plots. Lines represent three-exponential fits to the data, where χ^2_R is 1.7 (●) and 1.2 (○). Measurements were carried out using 0.3 mg mL^{-1} Er-ITC-labeled Ca-ATPase in buffer B [20 mM MES (pH 6.0), 20 mM $MgCl_2$, 20 mM K_2HPO_4, and 0.3 M sucrose] in the presence of either 0.1 mM $CaCl_2$ (●) or 1 mM EGTA (○). Frequency-domain errors in the measurement of the differential phase and modulated anisotropy were 0.2° and 0.005, respectively.

pholipid acyl chains, which are in contact with the Ca-ATPase (*59*). The activation energy of these protein-associated lipids [E_a(PALs)] can be estimated to be 5.8 ± 1.1 kcal mol^{-1}, where

$$E_a(\text{PALs}) = \frac{E_a(\text{SR}) - 0.57 \times E_a(\text{lipids only})}{0.43} \quad (4)$$

The similar activation energies associated with the rotational dynamics of the PALs and the Ca-ATPase (Figure 6A; E_a = 5.6 ± 0.5 kcal mol^{-1}) provide strong evidence that the measured 50 ± 10 μs correlation time (ϕ_2) corresponds to overall protein rotational motion about the membrane normal (Tables 2 and 3).

Protein−Protein Interactions between Ca-ATPase Polypeptide Chains. Calcium-induced alterations in the rotational dynamics of the phosphorylation domain (see above) may involve alterations in protein−protein interactions (*42*). Furthermore, temperature-dependent changes in protein−protein associations have been suggested to explain the large temperature dependence of enzyme activity and phosphoenzyme formation below 20 °C (*35*). Therefore, to detect possible alterations in protein−protein associations that may contribute to the observed changes in rotational dynamics, we have measured the steady-state fluorescence polarization (P) of FITC chromophores bound to adjacent Ca-ATPase polypeptide chains; a close proximity between FITC chromophores reduces P through FRET (*23*−*25*). A similar decrease in the emission anisotropy [$(1/P - 1/3)^{-1}$] is observed upon increasing the stoichiometry of FITC labeling at both 5 and 30 °C (Figure 7A). Calcium activation also results in essentially no difference in the anisotropy of FITC (data not shown). Together, these results suggest that there are no significant ligand- or temperature-dependent differences in association between Ca-ATPase polypeptide chains (Figure 7A). After disruption of oligomeric interactions between Ca-ATPase polypeptide chains by detergent solubilization, the emission anisotropy becomes independent of the labeling stoichiometry of FITC. These latter results are consistent with the specific labeling of a single site on each Ca-ATPase polypeptide chain, and indicate that the loss of anisotropy accompanying saturation of FITC sites in native SR membranes results from FRET between FITC chromophores bound to adjacent Ca-ATPase polypeptide chains (*16*, *24*). The small decrease in emission anisotropy following detergent solubilization at 30 °C in comparison to the results obtained at 5 °C suggests the presence of increased rotational dynamics at the higher temperature.

A quantitative consideration of the decrease in the emission anisotropy upon increasing the labeling stoichiometry of FITC indicates the presence of subunit interactions between Ca-ATPase polypeptide chains (Figure 7A; see eq 1 under Experimental Procedures). While the optimal fit to the data suggests that the average oligomeric state (N) of the Ca-ATPase in native SR membranes is a trimer or larger, earlier results have shown (i) that the Ca-ATPase functions as a dimer and ii) that nonspecific associations between Ca-ATPase polypeptide chains result in the formation of large aggregates (*34*, *35*, *47*, *60*, *61*). We have therefore fit the depolarization data to a two-state model involving dimers of the Ca-ATPase in equilibrium with higher molecular mass species (e.g., dodecamers) immobilized on the time-scale of our phosphorescence measurements, permitting an estimation of the maximal amount of nonspecific association within native SR membranes. Irrespective of the temperature, we find that less than 10% of Ca-ATPase species form higher molecular mass aggregates, and that there are no significant differences in protein−protein associations at 5 and 30 °C (Figure 7B). Thus, changes in the microsecond rotational

Table 3: Average Lifetimes and Anisotropy Decay Parameters for Er-ITC-Labeled Ca-ATPase[a]

sample	$<\tau>$ (μs)	r_0	g_1	ϕ_1 (μs)	g_2	ϕ_2 (μs)	g_3	ϕ_3 (μs)
				Buffer A[b] (pH 7.0)				
E[d] (EGTA)	302 (4)	0.37 (0.01)	0.62 (0.02)	4.7 (0.5)	0.20 (0.02)	47 (9)	0.18 (0.01)	900 (200)
E·Ca[e]	351$^+$ (18)	0.36 (0.01)	0.68$^+$ (0.01)	5.7 (0.5)	0.16* (0.01)	54 (10)	0.16 (0.01)	1300 (600)
E·ATP[f] (EGTA)	286 (5)	0.37 (0.01)	0.64 (0.01)	4.6 (0.4)	0.19 (0.01)	48 (8)	0.17 (0.01)	1200 (400)
				Buffer B[c] (pH 6.0)				
E−P[g] (EGTA)	277 (4)	0.35 (0.01)	0.62 (0.02)	5.3 (0.4)	0.20 (0.01)	69 (11)	0.18 (0.01)	1800 (600)
E·Ca[h]	277 (5)	0.35 (0.01)	0.68$^+$ (0.01)	6.2 (0.3)	0.14$^+$ (0.01)	67 (7)	0.18 (0.01)	1200 (200)

[a] Average phosphorescence lifetime and anisotropy decay parameters are derived from five to eight independent measurements. Numbers in parentheses are the associated standard errors of the mean. Significant differences are indicated at confidence levels of 90% (*) and 95% (+), as determined by the *F*-statistic. [b] Buffer A contains 35 mM MOPS (pH 7.0), 0.1 M KCl, 5 mM $MgCl_2$, and 0.3 M sucrose. [c] Buffer B contains 20 mM MES (pH 6.0), 20 mM $MgCl_2$, 20 mM K_2HPO_4, and 0.3 M sucrose. [d] Buffer A + 200 μM EGTA. [e] Buffer A + 100 μM $CaCl_2$. [f] Buffer A + 5 mM Mg·ATP + 200 μM EGTA. [g] Buffer B + 1 mM EGTA. [h] Buffer B + 100 μM $CaCl_2$.

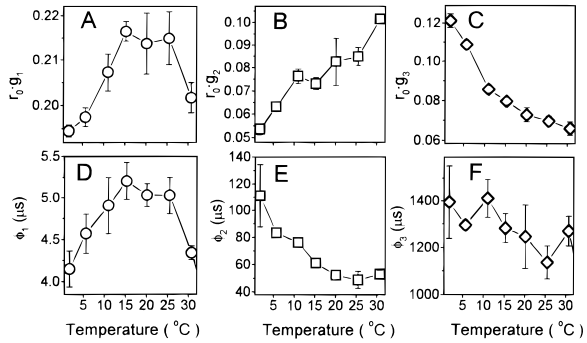

FIGURE 5: Temperature dependence of phosphorescence anisotropy decay parameters. Amplitudes (A−C) and rotational correlation times (D−F) are shown for Er-ITC-modified Ca-ATPase in buffer A in the presence of 0.1 mM $CaCl_2$. Error bars represent standard deviations of two independent measurements.

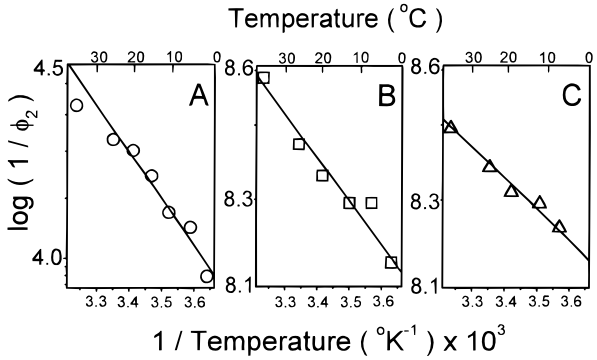

FIGURE 6: Arrhenius plots of protein and lipid rotational dynamics. Temperature-dependent changes in rotational correlation times of the Ca-ATPase (A) or membrane phospholipids either in native SR membranes (B) or in vesicles made from extracted SR lipids (C) were used to measure activation energies of rotational dynamics. Solid lines represent the best linear fits, whose activation energies and linear regression coefficients were (A) 5.6 ± 0.5 kcal mol^{-1} and 0.98 ± 0.03 for the Ca-ATPase (○), (B) 4.4 ± 0.5 kcal mol^{-1} and 0.97 ± 0.04 for SR membranes (□), and 3.3 ± 0.2 kcal mol^{-1} and 0.99 ± 0.02 for vesicles made from extracted SR lipids (△).

dynamics of Er-ITC associated with either calcium activation or temperature changes are largely the result of global structural rearrangements of the phosphorylation domain within a single Ca-ATPase polypeptide chain.

DISCUSSION

Summary of Results. High-affinity ATP binding and hydrolytic activities are retained following covalent attachment of the phosphorescent label Er-ITC to Lys_{464} within the phosphorylation domain (*12*), permitting the measurement of catalytically important global conformational changes involved in calcium transport. We find that calcium activation (E·Ca_2) increases large-amplitude domain motions of the phosphorylation domain in comparison to enzymatic states corresponding to the absence of bound ligands (E), the presence of bound nucleotide (E·ATP), or the phosphoenzyme intermediate (E−P) (Figure 4; Tables 2 and 3). In contrast, neither the average conformation nor the extent of protein−protein associations is significantly altered as a result of calcium activation. These results suggest an important role for dynamic structural changes of the phosphorylation domain in defining the vectorial transport mechanisms of the Ca-ATPase.

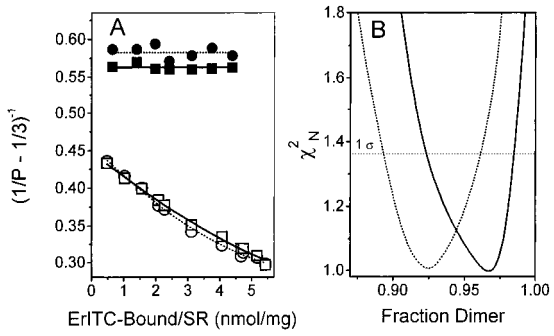

FIGURE 7: Relative proximity of Ca-ATPase polypeptide chains. (A) Steady-state emission anisotropy for FITC bound to the Ca-ATPase measured at 5 °C (○, ●) and 30 °C (□, ■) in the absence (○, □) or presence (●, ■) of 0.6 mM $C_{12}E_8$, where lines represent the least-squares fit to the data assuming FRET within a Ca-ATPase trimer (eq 1 under Experimental Procedures). (B) Error surfaces associated with fractional populations of Ca-ATPase dimers at 5 °C (dotted line) or 30 °C (solid line), assuming an equilibrium between dimers and dodecamers (eq 2 under Experimental Procedures). The horizontal line indicates one standard deviation. Experimental conditions involved 0.05 mg mL^{-1} SR in buffer A in the presence of 0.1 mM $CaCl_2$.

Relationship to Other Work. The nucleotide binding site is spatially distant from the sites for high-affinity calcium binding (*62*−*64*). However, while the long-range structural coupling between these distant sites is an essential feature with respect to the reaction mechanism (*2*), the details of the structural changes responsible for conformational coupling remain unclear. Local structural changes within the cytosolic domains and transmembrane helices of the Ca-ATPase that correlate with calcium activation and ATP utilization have been resolved using steady-state fluorescence measurements coupled with transient kinetic measurements using intrinsic or covalently bound spectroscopic probes (*63*,

65, *66*). Likewise, global conformational changes have been identified that are associated with (i) small alterations in the electron density of the cytosolic domains of the Ca-ATPase upon calcium activation and (ii) a large 8% redistribution of mass into the bilayer upon ATP-dependent phosphoenzyme formation (*67*−*70*). Consistent with the presence of global structural changes within the cytoplasmic portion of the Ca-ATPase upon enzyme phosphorylation, small alterations in the spatial arrangement between Ca-ATPase polypeptide chains have been resolved using FRET measurements (*42*). However, there are no large structural differences between the calcium-activated and phosphoenzyme forms of the Ca-ATPase that effect either the secondary structure, the molecular distances between chromophores located on Lys_{515} and Cys_{674}, or the average hydrodynamic properties of the Ca-ATPase with respect to the membrane normal (*42*, *71*−*76*). In contrast, large differences in the average conformation of the cytosolic domains are observed using image-enhanced electron microscopy for multilamellar crystals of the Ca-ATPase stabilized in the presence of 10 mM $CaCl_2$ compared with tubular crystals of the Ca-ATPase formed in the presence of 5 mM vanadate, which are expected to favor the formation of the two major conformational intermediates involved in the calcium transport mechanism (*7*, *9*). However, under these latter experimental conditions involving high calcium concentrations or the presence of a distribution of vanadate species, it is unclear how the resolved enzyme conformations relate to physiological intermediates important to the calcium transport mechanism since (i) multiple low-affinity calcium binding sites are occupied in the presence of millimolar concentrations of calcium and (ii) the presence of multiple species of vanadate exists in solution that may stabilize the Ca-ATPase in a conformation not present under physiological conditions (*9*). Using frequency-domain phosphorescence anisotropy to measure the rotational dynamics of the phosphorylation domain of the Ca-ATPase stabilized in different enzymatic states, we observe that neither calcium activation nor phosphoenzyme formation results in any significant differences in the rotational correlation time (ϕ_1) or normalized residual anisotropy (i.e., g_3) of the phosphorylation domain. Likewise, there are no ligand-dependent changes in the overall rate of rotational motion of the Ca-ATPase with respect to the membrane normal (ϕ_2), indicating that the average dimensions of the transmembrane portion of the Ca-ATPase are not altered (Table 3). Since changes in the average conformation of the phosphorylation domain would alter the residual anisotropy (*10*), these results indicate that the average conformation of the phosphorylation domain relative to the bilayer normal does not change appreciably upon calcium activation relative to other enzymatic states. Rather, calcium activation results in a larger amplitude of rotational motion within the phosphorylation domain of the Ca-ATPase (Figure 4; Table 3), suggesting that ligand binding primarily alters structural elements associated with interfacial regions between domain elements that function to modulate hingelike motions involving the two cytosolic domains of the Ca-ATPase. This latter suggestion is consistent with observed changes in the dimensions of the cytosolic stalk region upon calcium activation (*9*, *70*). It should be noted that our measurements do not resolve structural changes involving the nucleotide binding domain, and the large changes in the average structure observed in the presence of 10 mM $CaCl_2$ may therefore reflect changes in the average conformation of the nucleotide binding domain relative to the bilayer normal.

Physical Significance of Observed Calcium-Dependent Changes in Rotational Dynamics. The Ca-ATPase has been suggested to belong to a large superfamily of hydrolases that are structurally typified by L-2-haloacid dehalogenase (*77*). Structural elements that are spatially distant within the primary sequence create a conserved active site, which has been suggested to undergo a hingelike motion during catalysis in analogy to numerous water-soluble protein kinases (*3*, *4*, *6*, *78*). The arrangement of predicted secondary structural motifs within the cytoplasmic domain of the Ca-ATPase suggests the presence of distinct domains associated with phosphorylation and nucleotide binding, which may correspond to the two lobes resolved using image-enhanced electron microscopy (*6*, *9*, *79*). A cluster of short α-helices at the carboxyl terminal of the nucleotide binding domain is found in close contact with the phosphorylation domain, and has been proposed to form a hinge mediating interactions between the phosphorylation and nucleotide binding domains (*3*, *6*, *80*). The mutual destabilization between high-affinity calcium binding within transmembrane helices and the formation of the phosphoester intermediate at Asp_{351} in the phosphorylation domain forms the basis for coupling active calcium transport to ATP hydrolysis, which may involve a rigid structural linkage between the M4 transmembrane helix (Tyr_{294} to Thr_{316}) involved in calcium binding, the S4 stalk sequence (Thr_{317} to Lys_{329}), and the phosphorylation domain (*2*, *81*). It is therefore of interest to consider the physical significance of the observed structural changes involving the phosphorylation domain upon calcium activation. When modeled as motion within a cone, the amplitude of the rotational motion associated with the phosphorylation domain corresponds to a semiangle of approximately 44° (Tables 2 and 3) (*37*, *82*). This large amplitude of motion is consistent with rigid-body translocation of a domain about a hinge (*78*), and is comparable to what has previously been resolved in myosin, actin, immunoglobulins, dihydrofolate reductase, and T4 lysozyme (*37*, *38*, *83*−*88*). Phosphorylation or nucleotide binding to the Ca-ATPase results in no changes in the amplitude and rate of domain motion relative to apo-enzyme, suggesting that there are no alterations in the interaction between cytosolic domain elements. Upon calcium binding, the semiangle of the amplitude of the phosphorylation domain motion increases by 4 ± 1° (Table 3). This dynamic structural change may contribute to the structural coupling between the phosphorylation domain and the high affinity calcium binding sites located in the transmembrane helices. For example, previous work has shown that calcium activation results in a reorientation of transmembrane helices and associated structural changes near the bilayer surface (*7*, *9*, *70*, *89*, *90*), which may alter the stiffness of the collinear stalk region associated with the phosphorylation domain and thereby modulate the amplitude of domain motion. Thus, calcium-dependent structural changes may promote the transfer of the γ-phosphoryl group from ATP to form the phosphoester linkage and its subsequent hydrolysis. The reduced mobility of the phosphorylated enzyme intermediate in comparison to the calcium-activated form of the Ca-ATPase is furthermore consistent with earlier suggestions that phosphoenzyme formation is an entropy-driven reaction

facilitated by the displacement of water from the catalytic site, which stabilizes interactions between tertiary structural elements (*54*, *56*, *57*).

Conclusions and Future Directions. Large-amplitude motions of the phosphorylation domain involving structural elements in both the cytosolic and transmembrane regions of the Ca-ATPase are enhanced upon calcium activation (Figure 4). The structural linkage between cytosolic and transmembrane sequences provides a plausible physical mechanism to explain how calcium activation facilitates phosphoenzyme formation and hydrolysis. Thus, upon calcium binding the larger amplitudes associated with the domain motion of the phosphorylation domain are consistent with alterations in the structure of the stalklike region observed by image-enhanced electron microscopy (*9*), and may facilitate both ATP binding and transfer of the γ-phosphoryl group from ATP to form the phosphoester intermediate at Asp_{351}. However, the current results provide no information regarding possible changes in the average conformation of the nucleotide binding domain or regarding possible transient conformations in the enzymatic reaction mechanism. Future experiments should be directed at detecting kinetic intermediates and in defining additional labeling sites that permit the selective labeling and measurement of possible changes in the average conformation of the nucleotide binding domain for the Ca-ATPase stabilized in different enzymatic states.

REFERENCES

1. Rüegg, J. C. (1992) *Calcium in Muscle Contration*, pp 52−53, Springer-Verlag, New York.
2. Inesi, G. (1994) *Biophys. J. 66*, 554−560.
3. Taylor, W. R., and Green, N. M. (1989) *Eur. J. Biochem. 179*, 241−248.
4. Lacapère, J.-J., Garin, J., Trinnaman, B., and Green, N. M. (1993) *Biochemistry 32*, 3414−3421.
5. Toyoshima, C., Sasabe, H., and Stokes, D. L. (1993) *Nature 362*, 469−471.
6. MacLennan, D. H., Rice, W. J., and Green, N. M. (1997) *J. Biol. Chem. 272*, 28815−28818.
7. Zhang, P., Toyoshima, C., Yonekura, K., Green, N. M., and Stokes, D. L. (1998) *Nature* 392, 835−839.
8. Auer, M., Scarborough, G. A., and Kühlbrandt, W. (1998) *Nature 392*, 840−843.
9. Ogawa, H., Stokes, D. L., Sasabe, H., and Toyoshima, C. (1998) *Biophys. J. 75*, 51−52.
10. Cherry, R. J. (1992) in *The Structure of Biological Membranes* (Yeagle, P., Ed.) pp 507−537, CRC Press, Boca Raton, FL.
11. Kay, L. E., Muhandiram, D. R., Wolf, G., Shoelson, S. E., and Forman-Kay, J. D. (1998) *Nat. Struct. Biol. 5*, 156−163.
12. Huang, S., Negash, S., and Squier, T. C. (1998) *Biochemistry 37*, 6949−6957.
13. Fernandez, J. L., Rosemblatt, M., and Hidalgo, C. (1980) *Biochim. Biophys. Acta 599*, 552−568.
14. Folch, J., Lees, M., and Sloane Stanley, G. H. (1957) *J. Biol. Chem.* 226, 497−509.
15. Hidalgo, C., Ikemoto, N., and Gergely, J. (1976) *J. Biol. Chem. 251*, 4224−4232.
16. Mitchinson, C., Wilderspin, A. F., Trinnaman, B. J., and Green, N. M. (1982) *FEBS Lett. 146*, 87−92.
17. Squier, T. C., Mahaney, J. E., Yin, J.-J., Lai, C.-S., and Lakowicz, J. R. (1991) *Biophys. J. 59*, 654−669.
18. Lanzetta, P. A., Alverez, L. J., Reinsch, P. S., and Candia, O. (1979) *Anal. Biochem. 100*, 95−97.
19. Nicoli, D. F., McKenzie, D. C., and Wu, J.-S. (1991) *Am. Lab. 23*, 32−40.
20. Eads, T. M., Thomas, D. D., and Austin, R. H. (1984) *J. Mol. Biol. 179*, 55−81.
21. Sarna, T., and Sealy, R. C. (1984) *Photochem. Photobiol. 39*, 69−74.
22. Förster, T. (1948) *Ann. Phys. (Leipzig) 2*, 55−75.
23. Weber, G., and Daniel, E. (1966) *Biochemistry 5*, 1900−1907.
24. Highsmith, S., and Cohen, J. A. (1987) *Biochemistry 26*, 154−161.
25. Runnels, L. W., and Scarlata, S. F. (1995) *Biophys. J. 69*, 502−514.
26. Weber, G. (1981) *J. Phys. Chem. 85*, 949−953.
27. Lakowicz, J. R., Cherek, H., Maliwal, B. P., and Gratton, E. (1985) *Biochemistry 24*, 376−383.
28. Johnson, M. L., and Faunt, L. M. (1992) *Methods Enzymol. 210*, 1−37.
29. Lakowicz, J. R., and Gryczynski, I. (1991) *Topics in Fluorescence Spectroscopy* (Lakowicz, J. R., Ed.) Vol. 1, pp 293−336, Plenum Press, New York.
30. Beechem, J. M., Gratton, E., Ameloot, M., Knutson, J. R., and Brand, L. (1991) *Topics in Fluorescence Spectroscopy* (Lakowicz, J. R., Ed.) Vol. 2, pp 241−306, Plenum Press, New York.
31. Cobb, C. E., Hustedt, E. J., Beechem, J. M., and Beth, A. H. (1993) *Biophys. J. 64*, 605−613.
32. Carter, D. C., and Ho, J. X. (1994) *Adv. Protein Chem. 45*, 153−203.
33. Papp, S., Pikula, S., and Martonosi, A. (1987) *Biophys. J. 51*, 205−220.
34. Restall, C., Dale, R. E., Murray, E. K., Gilbert, C. W., and Chapman, D. (1984) *Biochemistry 23*, 6765−6776.
35. Birmachu, W., and Thomas, D. D. (1990) *Biochemistry 29*, 3904−3914.
36. Pilipovich, V. A. (1961) *Opt. Spectrosc. (USSR) 10*, 104−107.
37. Kinosita, K., Jr., Ishiwata, S., Yoshimura, H., Asai, H., and Ikegami, A. (1984) *Biochemistry 23*, 5963−5975.
38. Prochniewicz, E., Zhang, Q., Howard, E. C., and Thomas, D. D. (1996) *J. Mol. Biol. 255*, 446−457.
39. Prochniewicz, E., Zhang, Q., Janmey, P. A., and Thomas, D. D. (1996) *J. Mol. Biol. 260*, 756−766.
40. Sabbert, D., Engelbrecht, S., and Junge, W. (1997) *Proc. Natl. Acad. Sci. U.S.A. 94*, 4401−4405.
41. de Meis, L. (1988) *Methods Enzymol. 157*, 190−206.
42. Bigelow, D. J., Squier, T. C., and Inesi, G. (1992) *J. Biol. Chem. 267*, 6952−6962.
43. Anderson, N. G. (1966) *Natl. Cancer Inst. Monogr. 21*, 9−39.
44. Fajer, P., Knowles, F., and Marsh, D. (1989) *Biochemistry 28*, 5634−5643.
45. Hill, T. L., and Inesi, G. (1982) *Proc. Natl. Acad. Sci. U.S.A. 79*, 3978−3982.
46. Inesi, G., and Hill, T. L. (1983) *Biophys. J. 44*, 271−280.
47. Hymel, L., Maurer, A., Berenski, C., and Jung, C. Y. (1984) *J. Biol. Chem. 259*, 4890−4895.
48. Andersen, J. P. (1989) *Biochim. Biophys. Acta 988*, 47−72.
49. Mahaney, J. E., Froehlich, J. P., and Thomas, D. D. (1995) *Biochemistry 34*, 4864−4879.
50. Saffman, P. J., and Delbruck, M. (1975) *Proc. Natl. Acad. Sci. U.S.A. 72*, 3111−3113.
51. Squier, T. C., Bigelow, D. J., and Thomas, D. D. (1988) *J. Biol. Chem. 263*, 9178−9186.
52. Bigelow, D. J., Squier, T. C., and Thomas, D. D. (1986) *Biochemistry 25*, 194−202.
53. Asturias, F. J., Pascolini, D., and Blasie, J. K. (1990) *Biophys. J. 58*, 205−217.
54. Kanazawa, T. (1975) *J. Biol. Chem. 250*, 113−119.
55. Masuda, H., and de Meis, L. (1977) *J. Biol. Chem. 252*, 8567−8571.
56. de Meis, L. (1989) *Biochim. Biophys. Acta 973*, 333−349.
57. Schwarz, F. P., and Inesi, G. (1997) *Biophys. J.* 2179−2182.
58. Boctan, D. F., and Chan, S. I. (1978) *Annu. Rev. Phys. Chem. 29*, 307−335.
59. Squier, T. C., and Thomas, D. D. (1989) *Biophys. J. 56*, 735−748.
60. Squier, T. C., Hughes, S. E., and Thomas, D. D. (1988) *J. Biol. Chem. 263*, 9162−9170.

61. Voss, J., Jones, L. R., and Thomas, D. D. (1994) *Biophys. J. 67*, 190−196.
62. Squier, T. C., Bigelow, D. J., Fernandez-Belda, F. J., de Meis, L., and Inesi, G. (1990) *J. Biol. Chem. 265*, 13713−13720.
63. Bigelow, D. J., and Inesi, G. (1992) *Biochim. Biophys. Acta 1113*, 323−338.
64. Yonekura, K., Stokes, D., Sasabe, H., and Toyoshima, C. (1997) *Biophys. J. 72*, 997−1005.
65. Kanazawa, T., Suzuki, H., Daiho, T., and Yamasaki, K. (1995) *Biosci. Rep. 15*, 317−326.
66. Ferreira, S. T., and Coelho-Sampaio, T. (1996) *Biosci. Rep. 16*, 87−106.
67. Blasie, J. K., Herbette, L. G., Pascolini, D., Skita, V., Pierce, D., and Scarpa, A. (1985) *Biophys. J. 48*, 9−18.
68. Pascolini, D., and Blasie, J. K. (1988) *Biophys. J. 54*, 669−678.
69. Blasie, J. K., Pascolini, D., Asturias, F., Herbette, L. G., Pierce, D., and Scarpa, A. (1990) *Biophys. J. 58*, 687−693.
70. DeLong, L. J., and Blasie, J. K. (1993) *Biophys. J. 64*, 1750−1759.
71. Nakamoto, R. K., and Inesi, G. (1986) *FEBS Lett. 19*, 258−262.
72. Lewis, S. M., and Thomas, D. D. (1986) *Biochemistry 25*, 4615−4621.
73. Birmachu, W., Nisswandt, F. L., and Thomas, D. D. (1989) *Biochemistry 28*, 3940−3947.
74. Lewis, S. M., and Thomas, D. D. (1991) *Biochemistry 30*, 8331−8339.
75. Girardet, J. L., and Dupont, Y. (1992) *FEBS Lett. 296*, 103−106.
76. Baker, K. J., East, J. M., and Lee, A. G. (1994) *Biochim Biophys Acta 1192*, 53−60.
77. Aravind, L., Galperin, M. Y., and Koonin, E. V. (1998) *Trends Biochem. Sci. 23*, 127−129.
78. Subbiah, S. (1996) *Protein Motions*, R. G. Landes Co., Austin, TX.
79. MacLennan, D. H., Brandl, C. J., Korczak, B., and M., G. N. (1985) *Nature 316*, 696−607.
80. Møller, J. V., Juul, B., and le Maire, M. (1996) *Biochim. Biophys. Acta 1286*, 1−51.
81. Inesi, G., Lewis, D., Sumbilla, C., Nandi, A., Kirtley, M., and Ordahl, C. P. (1997) *Ann. N.Y. Acad. Sci. 834*, 207−220.
82. Kinosita, K. J., Kawato, S., and Ikegami, A. (1977) *Biophys. J. 20*, 289−305.
83. Bennett, W. S., and Huber, H. (1984) *Crit. Rev. Biochem. 15*, 291−384.
84. Lesk, A., and Chothia, C. (1988) *Nature 335*, 188−190.
85. Gerstein, M., Lesk, A. M., and Chothia, C. (1994) *Biochemistry 33*, 6739−6749.
86. Zhang, X.-J., Wozniak, J. A., and Matthews, B. W. (1995) *J. Mol. Biol. 250*, 527−552.
87. Bahar, I., Erman, B., Haliloglu, T., and Jernigen, R. L. (1997) *Biochemistry 36*, 13512−13523.
88. Mchaourab, H., Oh, K. J., Fang, C. J., and Hubbell, W. L. (1997) *Biochemistry 36*, 307−316.
89. Gryczynski, I., Wiczk, W., Inesi, G., Squier, T., and Lakowicz, J. R. (1989) *Biochemistry 28*, 3490−3498.
90. Asturias, F. J., Fischetti, R. F., and Blasie, J. K. (1994) *Biophys. J. 66*, 1665−1677.
91. Steiner, R. F. (1991) *Topics in Fluorescence Spectroscopy* (Lakowicz, J. R., Ed.) Vol. 2, pp 1−52, Plenum Press, New York.
92. Cantor, C. R., and Schimmel, P. R. (1980) *Biophysical Chemistry. Part II: Techniques for the study of biological structure and function*, W. H. Freeman and Co., San Francisco.
93. Weast, R. C. (1961) *Handbook of Chemistry and Physics*, 43rd ed., p 2227, The Chemical Rubber Co., Cleveland, OH.

BI981997+